



# Network Patterns of Beta-Amyloid Deposition in Parkinson's Disease

Jinhee Kim<sup>1,2</sup> · Christine Ghadery<sup>1,2</sup> · Sang Soo Cho<sup>1,2</sup> · Alexander Mihaescu<sup>1,2,3</sup> · Leigh Christopher<sup>1,2</sup> · Mikaeel Valli<sup>1,2,3</sup> · Sylvain Houle<sup>1</sup> · Antonio P. Strafella<sup>1,2,3,4</sup>

Received: 24 January 2019 / Accepted: 24 April 2019 / Published online: 20 May 2019  
© Springer Science+Business Media, LLC, part of Springer Nature 2019

## Abstract

Beta-amyloid (A $\beta$ ) in the brain is a key pathological feature of certain neurodegenerative diseases. Recent studies using graph theory have shown that A $\beta$  brain networks are of pathological significance in Alzheimer's disease (AD). However, the characteristics of A $\beta$  brain networks in Parkinson's disease (PD) are unknown. In the present study using positron emission tomography (PET) with [<sup>11</sup>C]-Pittsburgh compound B (PiB), we applied a graph theory-based analysis to assess the topological properties of A $\beta$  brain network in PD patients with and without A $\beta$  burden (PiB-positive and PiB-negative, respectively) and healthy controls with A $\beta$  burden. We found that the PD PiB-positive group demonstrated significantly lower value in global efficiency and modularity compared with PD PiB-negative group. The less robust modular structure indicates the tendency of having increased *inter-modular* connections than *intra-modular* connectivity (i.e., reduced segregation). Results of hub organization showed that relative to PD PiB-negative group, different hubs were identified in the PiB-positive group, which were located mainly within the default mode network. Overall, our findings suggest disturbances in A $\beta$  topological organization characterized by abnormal network integration and segregation in PD patients with A $\beta$  burden. The stronger *inter-modular* connectivity observed in the PD PiB-positive group may suggest the spreading pattern of A $\beta$  between modules in those PD patients with elevated PiB burden, thus providing insight into the beta-amyloidopathy of PD.

**Keywords** Parkinson's disease · Beta-amyloid · Pittsburgh compound B positron emission tomography (PiB-PET) · Graph theory

## Introduction

Parkinson's disease (PD) is the second most common neurodegenerative diseases after Alzheimer disease (AD) and is considered to be a multi-system disorder combining progressive motor and cognitive impairment [1, 2]. Along with

cortical Lewy body and neurites deposition [3], fibrillary beta-amyloid (A $\beta$ ) plaques, have been identified as the neuropathological correlates in PD patients with cognitive decline [4]. One of the imaging biomarkers for assessing A $\beta$  deposition in vivo is the radiotracer carbon 11-labeled Pittsburgh compound B ([<sup>11</sup>C] PiB) [5, 6]. In previous studies utilizing amyloid PET imaging, patients with PD rarely exhibited the AD range of elevated A $\beta$  burden [7–9]. However, other studies have reported that A $\beta$  deposition in patients with PD may be associated with future worsening of cognitive performance [10, 11], indicating the clinical relevance of A $\beta$  burden in patients with PD. A recent study using a principal component analysis demonstrated that patients with PD have cortical PiB-binding patterns distinct from AD, suggesting a different A $\beta$  pathological contribution in PD [12].

Moving beyond regional pathology, there is an increasing number of studies investigating the effects of A $\beta$  deposition on whole-brain networks. Brain network analysis based on the graph-theoretical methods enables us to investigate the underlying communication between different brain regions [13, 14], measuring complex topological properties, such as global integration (i.e., ability to transfer information to distant

✉ Jinhee Kim  
jin-hee.kim@camhpet.ca

<sup>1</sup> Research Imaging Centre, Campbell Family Mental Health Research Institute, Centre for Addiction and Mental Health, University of Toronto, Toronto, Ontario, Canada

<sup>2</sup> Division of Brain, Imaging and Behaviour – Systems Neuroscience, Krembil Research Institute, University Health Network, University of Toronto, Toronto, Ontario, Canada

<sup>3</sup> Institute of Medical Science, University of Toronto, Toronto, Ontario, Canada

<sup>4</sup> Morton and Gloria Shulman Movement Disorder Unit and E.J. Safra Parkinson Disease Program, Neurology Division, Department of Medicine, Toronto Western Hospital, University Health Network, University of Toronto, Toronto, Ontario, Canada

connections) and local segregation (i.e., capacity for specialized processing). To date, there have been few PET imaging studies which assessed A $\beta$  networks constructed from regional A $\beta$  deposition in individuals with mild cognitive impairment and AD patients [15–18]. Pereira et al. [18] examined the properties of an A $\beta$  network in non-demented participants with different stages of A $\beta$  accumulation and proposed a potential use of topological patterns for assessing the progression of AD during the preclinical/clinical stages.

In PD patients, the impact of the A $\beta$  networks and the contribution of A $\beta$  burden to network abnormality have not been investigated yet. In this paper, we applied the graph theoretical analysis to construct an A $\beta$  brain network model that accounted for correlations between regional cortical A $\beta$  retention binding obtained from [ $^{11}\text{C}$ ] PiB-PET scans. Our main goal was to explore the effect of beta-amyloid pathology on the organization of the beta-amyloid networks in PD. Our rationale was that as the pattern of amyloid PET binding in PD is apparently distinct from AD [12], properties of the A $\beta$  brain network in patients with PD could be indeed different from that of AD.

## Materials and Methods

### Participants and Study Design

In total, 30 patients with PD (mean  $\pm$  SD, 65.43  $\pm$  6.35 years; eight female) with and without A $\beta$  deposits along with 16 healthy controls (HC; mean  $\pm$  SD, 64.31  $\pm$  7.99 years; 11 female) with A $\beta$  deposits were identified according to criteria specified below. The diagnosis of idiopathic PD was made based on the UK Brain Bank criteria [19]. Exclusion criteria included a history of head injury, psychiatric or other neurological diseases, and alcohol or drug dependency or abuse. All participants were screened for MRI compatibility. Patients with PD were asked to withdraw from anti-parkinsonian medication for 12 h prior to [ $^{11}\text{C}$ ] PiB-PET imaging scans. The high-resolution T1-weighted and proton density-weighted structural MRI scans were performed on a separate day to minimize excessive fatigue. The experimental procedures were explained to participants, and written informed consent was obtained prior to study participation. The study was approved by the Centre for Addiction and Mental Health Research Ethics Board.

Disease severity was assessed in patients with PD using the motor subset of the Unified Parkinson Disease Rating Scale (UPDRS) and Hoehn and Yahr (H-Y) stages. Levodopa equivalent daily dose (LEDD) was calculated for each patient in accordance with a previous study [20]. The averaged LEDD across the PD patients was 732.28  $\pm$  425.91 mg. The Montreal Cognitive Assessment (MoCA) was used to evaluate the overall cognitive performance. We measured the

depression symptoms of subjects using the Beck Depression Inventory-II (BDI-II) [21]. Demographic and clinical characteristics are listed in Table 1.

### MRI Data Acquisition

For each participant, proton density-weighted brain MRI images were obtained with the following parameters: oblique plane, 84 slices; matrix of 256  $\times$  192; 22 cm FOV; 2.0-mm slice thickness; TE = Min Full; TR = 6000 ms; flip angle = 90°. The MRI images were used for co-registration with the [ $^{11}\text{C}$ ] PiB-PET scan, segmentation, and region of interest (ROI) delineation. Structural MRI data were collected on a 3-T GE Discovery MR 750 scanner with an eight-channel radio frequency head coil: a fast-spoiled gradient echo pulse sequence; repetition time = 6.7 ms; echo time = 3.0 ms; flip angle = 8°; field of view = 230  $\times$  230 mm<sup>2</sup>; matrix size = 256  $\times$  256  $\times$  200; sagittal slices; and voxel size = 0.89  $\times$  0.89  $\times$  0.9 mm<sup>3</sup>.

### PET Data Acquisition and Preprocessing

The [ $^{11}\text{C}$ ] PiB-PET scans were obtained using the Siemens high-resolution research tomograph (HRRT) scanner. It measures radioactivity in 207 brain sections with a 1.22-mm thickness. To minimize participant head movement during the scan, custom-made thermoplastic face masks together with a head-fixation system (Tru-Scan Imaging) were used. A 10-min transmission scan with a single photon point source  $^{137}\text{Cs}$  ( $t_{1/2}$  = 30.2 years,  $E_{\gamma}$  = 662 keV) was obtained before the emission scan for the correction of photon attenuation. To measure levels of A $\beta$  burden, participants were given a bolus injection of [ $^{11}\text{C}$ ] PiB with the radioactive tracer (mean  $\pm$  SD; 9.64  $\pm$  0.86 mCi) into an intravenous line placed in an antecubital vein and underwent a 90-min scan at rest. PET images were reconstructed into a series of 34 frames consisting of 4  $\times$  15 s, 8  $\times$  30 s, 9  $\times$  60 s, 2  $\times$  180 s, 8  $\times$  300 s, and 3  $\times$  600 s.

Preprocessing of PET data were performed using ROMI, an in-house automated software [22] and Statistical Parametric Mapping software (SPM8; Wellcome Department of Imaging Neuroscience, London, UK). As previously described [22], a standard brain template (International Consortium for Brain Mapping/Montreal Neurological Institute 152 MRI) containing the predefined region of interests (ROIs) was non-linearly transformed to fit the individual high-resolution proton density-weighted MRI. The resulting individual ROIs were aligned and re-sliced to match the PET images using a normalized mutual information algorithm. For ROI analysis, 24 cortical ROIs (12 for each hemisphere) were delineated based on standardized stereotaxic space [23].

**Table 1** Demographic and clinical characteristics of the patients with Parkinson's disease

	PD PiB-negative ( <i>n</i> = 14)	PD PiB-positive ( <i>n</i> = 16)	HC PiB-positive ( <i>n</i> = 16)
Sex (M/F)	12 M, 2 F	10 M, 6 F	5 M, 11 F
Age	65.86 ± 4.90	65.06 ± 7.54	64.31 ± 7.99
MoCA	25.00 ± 3.72	25.56 ± 2.99 <sup>b</sup>	27.44 ± 1.50
Education (years)	14.86 ± 3.18	15.94 ± 3.59	16.50 ± 3.08
BDI-II <sup>a</sup>	10.5 ± 9.33	8.00 ± 5.84 <sup>b</sup>	3.07 ± 4.57
LEDD	818.77 ± 446.99	662.00 ± 408.67	–
UPDRS-III	41.64 ± 30.65 (13–93)	29.25 ± 16.69 (10–78)	–
H-Y stage	2.03 ± 0.50 (1.5–4)	2.36 ± 0.63 (1.5–3)	–
[ <sup>11</sup> C]-PiB			
Amount injected (mCi)	9.78 ± 0.85	9.51 ± 0.63	9.72 ± 1.06
Specific activity (mCi/μmol)	1610.18 ± 668.49	2003.49 ± 878.27	2016.25 ± 972.67
Mass injected (μg)	1.87 ± 0.81	1.68 ± 1.33	1.61 ± 1.02

Mean ± SD and range (min.–max.). Statistical significance was determined by a two-sample *t* test for age, MoCA, BDI, and chi-square test for gender difference

MoCA Montreal Cognitive Assessment, UPDRS-III Unified Parkinson's Disease Rating Scale III, LEDD levodopa equivalent daily dose, SD standard deviation

<sup>a</sup> BDI data missing for one subject

<sup>b</sup> Significant group difference between PD PiB-positive and HC PiB-positive group at *P* < 0.05

[<sup>11</sup>C]-PiB retention was expressed as the distribution volume ratio (DVR) representing fibrillar Aβ burden [5] using the Logan graphic method [24]. The cerebellum was used as a reference region since it is devoid of significant levels of fibrillar Aβ in PD [25]. The simplified reference tissue model has been shown to be an appropriate model for quantifying [<sup>11</sup>C] PiB data in humans without arterial input function [26]. The kinetic analysis of [<sup>11</sup>C] PiB was performed using PMOD 3.6 modeling software (PMOD Technologies Ltd., Zurich, Switzerland). The [<sup>11</sup>C] PiB index was calculated by averaging DVR values from the cortical regions including prefrontal, inferior parietal cortex, precuneus, and occipital cortex [27]. Patients with PD were classified into two groups based on the [<sup>11</sup>C] PiB index with the cut-off of 1.08, which was suggested as the optimal cut-point with high sensitivity without compromising specificity (sensitivity, 95.5%; specificity, 81%) [28]. For the HC group, one participant classified as PiB-negative was excluded for further analysis, resulting in all 16 HCs as PiB-positive.

### Network Construction: Node and Edge Definition

We applied a graph theory approach to examine the topological organization of the Aβ network constructed from regional Aβ deposition (Fig. 1a) using the brain connectivity toolbox [29] and the graph analysis toolbox (GAT) [30]. In the Aβ network, nodes represent predefined 24 bilateral cortical ROIs. The names of the ROIs are listed in Table 2. Edges denote the linear correlation between Aβ DVR values of every pair of nodes as quantified with a Pearson correlation. The Aβ brain network was built for each PD group, wherein the inter-regional correlation matrix was

calculated across individuals in each PD group. This network construction method has been widely used in previous studies [17, 31, 32]. In brief, edges of each group's Aβ network indicate how much amyloid retention of one brain region correlated with that of another brain region across individuals, representing similarity of Aβ burden.

Adopting the simple network model, which is an undirected and unweighted graph, the adjacency binary matrix (i.e., defining the topology of the network) was generated, in which edges were designated as 1 if an edge existed between two nodes that was larger than the selected threshold, and 0 otherwise. For group comparison, to ensure that the groups had the same number of edges, we used the range of the sparsity threshold from 0.1 to 0.34 in 0.03 intervals [33]. More specifically, sparsity denotes the ratio of the number of actual edges divided by the total possible number of edges ( $N(N-1)/2$ ;  $N_{\text{nodes}} = 24$ ). A minimum sparsity of 10% was selected, considering the number of edges which is superior to the number of nodes. Matrix thresholded at the sparsity 31% is represented in a connectogram along with the ROI spatial maps (Fig. 1b) and modular graph labeled by four subnetworks (Fig. 1c). We focused on the group difference on graph metrics within the small-world regime, wherein groups also showed the small-worldness properties with a range of  $\sigma > 1$ . Only the positive values of the edges were considered.

### Topological Analysis

We characterized the topology of Aβ network by focusing on (1) the ability to integrate information between distant brain

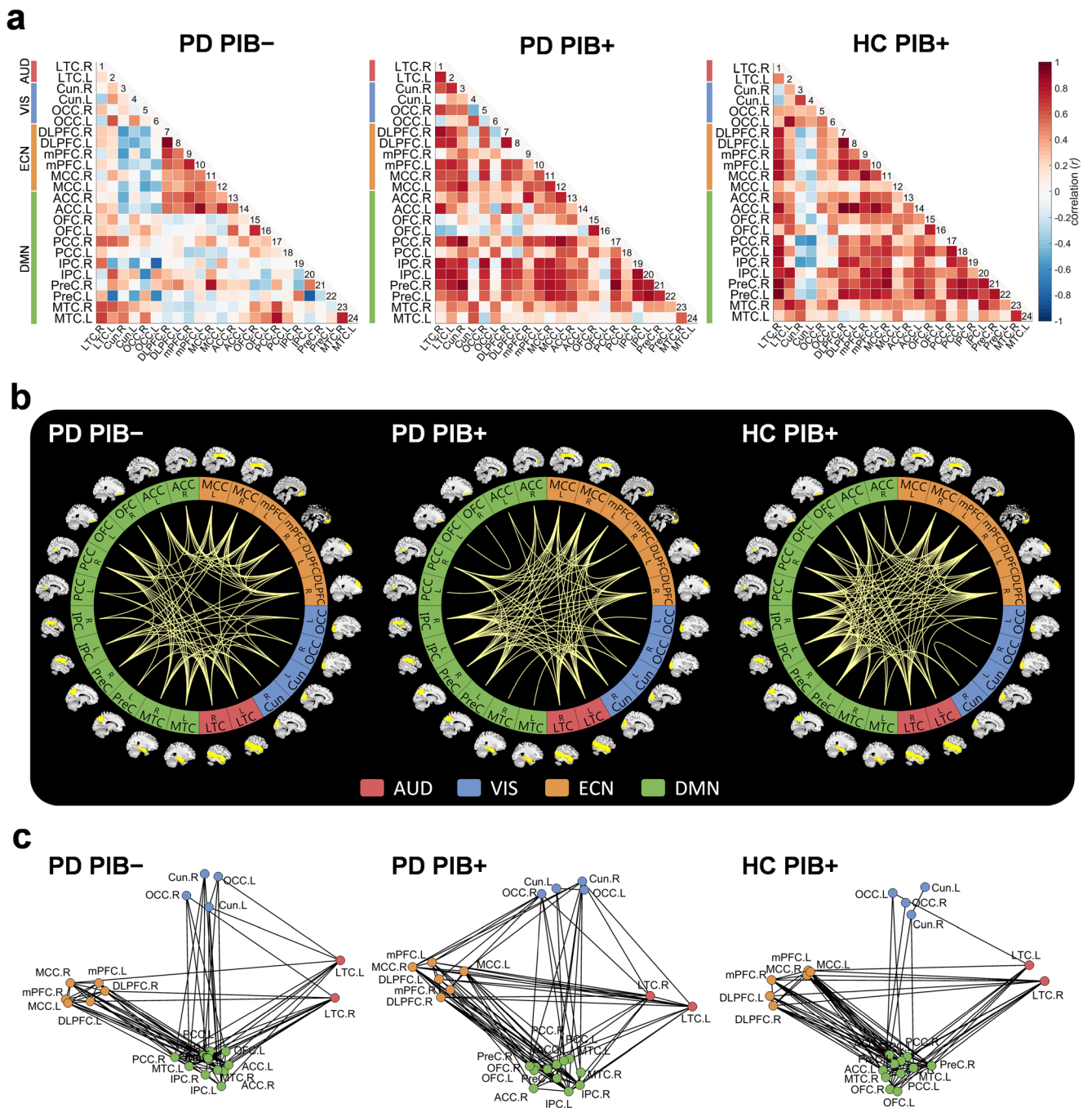


**Fig. 1** The characteristics of A $\beta$  network in PD PiB-negative (PD PiB $^-$ ), PD PiB-positive (PD PiB $^+$ ), and HC PiB-positive (HC PiB $^+$ ), respectively. **a** The Pearson correlation matrices of A $\beta$  retention between 24

regions. Matrices at a sparsity 31% are shown in circular structure plot (**b**) and four subnetwork-based modular graphs (**c**). Each square color represents one of the networks, such as AUD, VIS, ECN, and DMN

regions (network integration: global efficiency), (2) the capacity for integrated processing within densely interconnected groups of regions (network segregation: local efficiency, clustering coefficient, and modularity), and (3) hub organization (importance of the nodes: degree and betweenness centrality).

First, we assessed the global network properties or the network integration of A $\beta$  networks by calculating global efficiency which was computed as the average of the inverse of

the shortest path length (i.e., number of links) between each pair of all nodes [34]. Brain networks with high efficiency indicate that pairs of nodes have short communication distance; that is, few steps are needed to reach each other, enabling efficient global information transfer. Secondly, we included local efficiency, clustering coefficient, and modularity metric to assess network segregation, that is, local connectivity properties. Local efficiency is defined as the inverse of the

**Table 2** Twenty-four nodes and its abbreviations

Index	Brain networks	Regions (full name)	Abbreviations	MNI coordinates		
				x	y	z
1	AUD	Lateral temporal cortex	LTC.R	53	−28	−5
2			LTC.L	−52	−28	−5
3	VIS	Cuneus	Cun.R	14	−87	15
4			Cun.L	−12	−87	15
5	VIS	Occipital cortex	OCC.R	37	−84	1
6			OCC.L	−36	−84	1
7	ECN	Dorsolateral prefrontal cortex	DLPFC.R	23	48	30
8			DLPFC.L	−23	48	30
9	ECN	Medial prefrontal cortex	mPFC.R	7	45	2
10			mPFC.L	−7	45	2
11	ECN	Middle cingulate cortex	MCC.R	10	−13	37
12			MCC.L	−9	−13	37
13	DMN	Anterior cingulate cortex	ACC.R	9	41	5
14			ACC.L	−8	41	5
15	DMN	Orbitofrontal cortex	OFC.R	24	44	−18
16			OFC.L	−24	44	−18
17	DMN	Posterior cingulate cortex	PCC.R	10	−56	13
18			PCC.L	−9	−56	13
19	DMN	Inferior parietal cortex	IPC.R	54	−24	27
20			IPC.L	−52	−24	27
21	DMN	Precuneus	PreC.R	15	−65	41
22			PreC.L	−14	−65	41
23	DMN	Mesial temporal cortex	MTC.R	26	−20	−18
24			MTC.L	−27	−19	−18

The odd index represents the right hemisphere while the even index for the left hemisphere. The coordinate information was calculated by the center of mass for each region

AUD auditory network, VIS visual network, ECN executive cognitive network, DMN default mode network, L left, R right

shortest path length in subgraph which are neighbors with the corresponding node, indicating the efficiency of information exchange between subgraphs [34]. It is considered to measure the fault tolerance of the network, that is, the efficiency of the communication within the neighbors of a node<sub>*i*</sub> when the node<sub>*i*</sub> is removed [33]. The clustering coefficient of the node was defined as the density of connections between the node's neighbors [35]. Brain networks with higher averaged clustering coefficients have densely interconnected neighbors, that is, a cluster, respecting the greater local segregation. In addition, we estimated modularity index which reflects the extent of how a network is organized into a modular structure, in which the nodes are densely connected with each other while sparsely connected with the nodes of other modules [36].

Lastly, we assessed the relevance of the nodes in the network. The nodal characteristics were computed for the degree and the betweenness centrality (Be) to examine highly connected regions (i.e., hub) of the Aβ brain network. The degree is defined as the number of edges in a node. Betweenness

centrality of a node *i* (Be<sub>*i*</sub>) is defined as the fraction of all shortest paths that run through a given node<sub>*i*</sub> [37]. A node with high Be<sub>*i*</sub> indicates that information needs to go through the node, enabling control of information flow. Hubs are considered crucial components for facilitating the global integrative process in a brain network, either by having abundant connections to another node or by being a shortcut path to other nodes. Therefore, both degree and Be<sub>*i*</sub> were used to identify hubs in Aβ network. Nodes with a degree or Be greater than one standard deviation above the average of all nodes in the network were regarded as hubs [38].

## Statistical Analyses

Statistical significance of the group difference in demographic and clinical measurement was determined using two-sample *t* tests and chi-square tests in SPSS software (Version 20.0; IBM Corp. Armonk, NY, USA). For the network analysis, a non-parametric permutation test was applied to determine the

statistical significance of between-group differences. First, participants of two groups were randomly assigned to one of the groups. Using the new randomized data set, all graph measurements were calculated. This randomization procedure was repeated 5000 times to produce the distribution of the inter-group difference in the topological metrics as a function of sparsity. The 95th confidence intervals of the distribution were used as the critical values for a one-tailed test ( $P < 0.05$ ). The rejection of the null hypothesis indicates that the observed topological parameter difference of the A $\beta$  network between the two groups is significant. To examine the group comparison for each topological metric, we applied additional analyses, such as an area under the curve (AUC) approach as well as functional data analyses (FDA) as implemented in GAT [30]. These methods are widely used for avoiding a specific selection of a thresholding process in graph theory-based network studies [38, 39]. The AUC is the definite integral within the defined sparsity threshold range. Additionally, FDA,

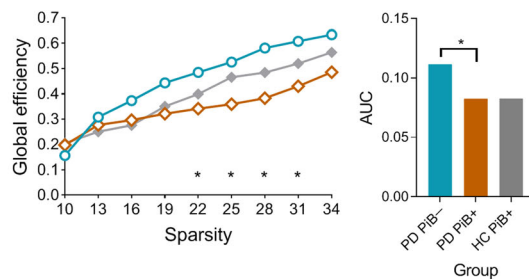
depicted as the summation of curves over the sparsity threshold range [40], was also adopted because of hypersensitivity of AUC at higher network sparsity and insensitivity to differences in the curve shape rather their mean [30].

## Results

### Demographic and Clinical Characteristics

Detailed demographic and clinical information are shown in Table 1. There were no significant differences between PiB-positive and PiB-negative PD groups in terms of sex ( $\chi^2(1) = 2.058$ ,  $P = 0.151$ , chi-square test), age ( $t(28) = -0.337$ ,  $P = 0.739$ , two-sample  $t$  test), and years of education ( $t(28) = 0.867$ ,  $P = 0.393$ , two-sample  $t$  test). We also did not find any group difference in cognitive impairment (MoCA;  $t(28) = 0.459$ ,  $P = 0.650$ , two-sample  $t$  test) and depression

#### a Global network properties



#### b Local network properties

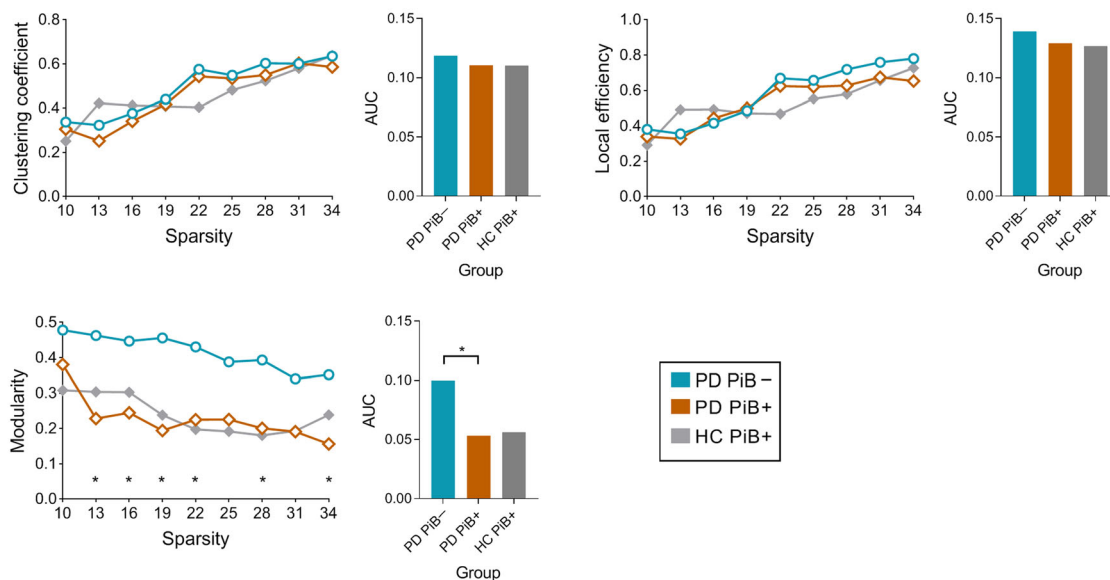


**Fig. 2** Topological measurements of the A $\beta$  network for the two PD groups and the HC PiB-positive group as a function of sparsity and integrated AUC results. **a** Global network property: global efficiency. **b** Local network properties: local efficiency, clustering

coefficient, and modularity. Asterisk indicates that there is a significant group difference between PD PiB-positive [PD PiB+] and PD PiB-negative group [PD PiB-]

symptom (BDI-II;  $t(28) = -0.892$ ,  $P = 0.280$ , two-sample  $t$  test). Compared with the HC group, PiB-positive PD group exhibited a lower general cognitive function measured by MoCA ( $t(30) = 2.24$ ,  $P = 0.033$ ) and a higher depressive symptom ( $t(29) = -2.61$ ,  $P = 0.014$ ).

### Altered Network Integration and Segregation Properties of the A $\beta$ Networks in PD PiB-Positive Group

Figure 2 shows the results of the network metrics over the entire threshold range. Statistical analyses as a function of the sparsity revealed that global efficiency was significantly lower in the PiB-positive group than the PiB-negative group at sparsity values of 22–31% ( $P < 0.05$ ); i.e., lower global efficiency indicated that pairs of nodes had longer communication distances, that is, longer paths between nodes.

Among the network segregation measurements, a significant group difference was only found in the modularity. More specifically, the PiB-positive group compared with the PiB-negative group had a lower modularity value in a certain sparsity range; 13–22%, 28%, and 34%, i.e. reflecting that the extent of the modular structure (nodes densely connected with each other while sparsely connected with the nodes of other modules) was less preserved. There was no statistically significant group difference over the entire threshold range for a mean clustering coefficient and local efficiency.

Like the sparsity-dependent statistical analysis results, a significant group difference was confirmed in the global efficiency and modularity by the AUC and FDA analyses. Again, the PiB-positive group showed reduced global efficiency values ( $P_{AUC} = 0.034$ ;  $P_{FDA} = 0.039$ ) and less optimal modular structures ( $P_{AUC} = 0.021$ ;  $P_{FDA} = 0.034$ ). Altogether, these observations suggest that the PD-positive A $\beta$  network is associated with relatively sparse intra-modular connections (i.e., reduced network integration) and relatively stronger inter-modular connections (i.e., impaired network segregation) (Fig. 1).

As expected, the HC PiB-positive group presented a similar trend of the PD PiB-positive group, but global efficiency and modularity did not significantly differ between the PD PiB-negative group and the HC PiB-positive group (Fig. 2), suggesting that together, neurodegeneration (e.g., alpha-synuclein deposition) and A $\beta$  burden may play an additive and complementary contribution in affecting network connectivity.

### Hub Organization of the A $\beta$ Networks

We examined the hub organization in A $\beta$  network between groups. Hubs are considered a crucial component for facilitating the global integrative process in a brain network, either by having abundant connections to another node or by being a

shortcut path to other nodes. Table 3 illustrates hubs for each group based on the nodal degree and betweenness centrality. Spatial distribution for hubs in the two groups displayed was different. Network hubs for the PD PiB-positive group were found mainly in the default mode network (DMN) and executive cognitive network (ECN). Significantly different hubs in the PD PiB-positive group (compared with the PD PiB-negative) were found in the bilateral inferior parietal cortex (FDR-corrected  $P < 0.05$  across 24 brain regions; Fig. 3).

## Discussion

In the current study, we used network-based analysis to examine the characteristics of the A $\beta$  network and the impact of elevated A $\beta$  burden in PD patients. We demonstrated that the A $\beta$  network of PD PiB-positive patients was characterized by altered topological architectures with a reduction in global efficiency as well as modularity, indicating impaired network integration and neural segregation.

Regional A $\beta$  accumulation in non-demented PD patients is known to increase with age [11] and is sometimes associated with more advanced stages of PD [41]. However, we did not find any significant differences between the PD PiB-positive and PiB-negative groups in terms of age and PD severity. Thus, it is unlikely that the abnormal A $\beta$  network was relatively dependent on aging and disease progression.

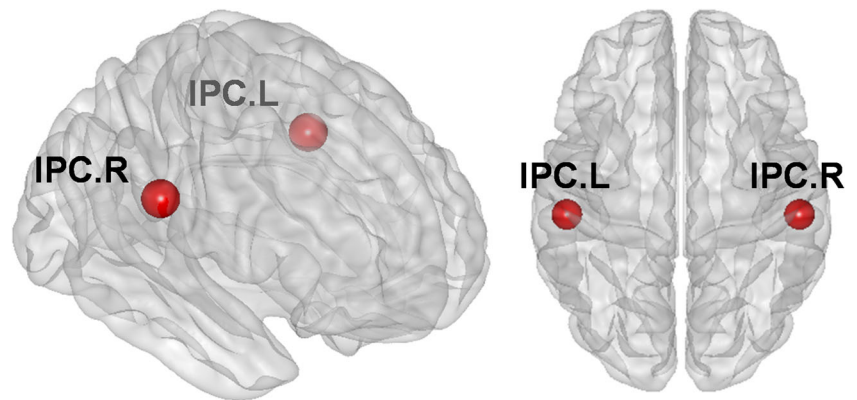
**Table 3** Hubs and nodal characteristics in PD PiB-positive and PD PiB-negative groups

Region	L/ R	Brain networks	Be <sub><i>i</i></sub>	Degree
PD PiB-positive group				
Inferior parietal cortex*	L	DMN	9.1	9.1
	R	DMN	4.2	8.4
Posterior cingulate cortex	R	DMN	9.0	7.0
Middle cingulate cortex	L	ECN	8.1	6.3
	R	ECN	2.9	7.7
Dorsolateral prefrontal cortex	R	ECN	6.5	7.0
Precuneus	R	DMN	2.9	7.7
PD PiB-negative group				
Lateral temporal cortex	R	AUD	9.1	8.0
	L	AUD	5.7	6.9
Posterior cingulate cortex	R	DMN	5.1	8.0
Middle cingulate cortex	R	ECN	3.9	9.7

\* Brain region that significantly changed in the PD PiB-positive group compared with the PD PiB-negative group (at FDR-corrected  $P < 0.05$  across 24 brain nodes)

Be<sub>*i*</sub>, betweenness of a node *i*, DMN default mode network, ECN executive cognitive network, AUD auditory network, L left, R right

**Fig. 3** Group difference in hubs between PD PiB-positive and PD PiB-negative. Red circle indicates brain regions showing increased nodal characteristics in PD PiB-positive relative to PD PiB-negative group. IPL.R right inferior parietal lobe, IPL.L left inferior parietal lobe



The reduced global efficiency found in the PD PiB-positive group indicates that the A $\beta$  network in these patients was associated with poor information transfer in long-distance connections. Similar findings have been reported in previous PiB studies of AD [16, 42, 43], which found either decreased efficiency or longer path. This is a compelling observation because aggregation of A $\beta$  may spread across brain regions with direct neuronal connections [44].

In the current study, a significant group difference for network segregation properties was found only in the modularity, but not in clustering coefficient and local efficiency. This is consistent with the previous findings suggesting that the clustering coefficient is less affected than global efficiency in the early stage of A $\beta$  accumulation [18]. Modularity index reflects the extent of how a network is organized into a modular structure in which the nodes belonging within the same module are densely connected with each other while sparsely connected with the nodes of another module. The PD PiB-positive group demonstrated a less robust modular structure, indicating the tendency having increased *inter-modular* connections than *intra-modular* connections (i.e., reduced segregation). The stronger inter-modular connectivity observed in the PD PiB-positive group may suggest the spreading pattern of A $\beta$  between modules in PD patients with elevated PiB burden.

Brain regions characterized by higher connection with other nodes or bridging between nodes are considered hubs in network analysis [45]. Those hubs regions were suggested to play a putative role in A $\beta$  spreading, as observed in a previous PiB-PET imaging study [46]. Despite having shared hubs with PD PiB-negative group, different hubs were also identified in the A $\beta$  network of the PD PiB-positive group located primarily in hetero-modal associations area overlapping with the DMN. These findings are consistent with the previous evidence of regional A $\beta$  network abnormality in DMN [18]. These new hubs of the PD PiB-positive group were found in the bilaterally inferior parietal cortex, a region known to be involved in cognitive tasks of visuomotor integration and

visuospatial performance [47, 48]. This restructuring of the hub organization may represent a biomarker of a cognitive compensatory mechanism in PD.

The HC PiB-positive group showed a trend in global efficiency and modularity similar to PD PiB-positive but did not differ significantly from the PD PiB-negative group. This observation suggests that both the neurodegenerative process (i.e., alpha-synuclein deposition) and A $\beta$  burden may play an additive and complementary role in affecting the A $\beta$  network organization. Future studies with longitudinal cohort data are needed to properly demonstrate the effect of amyloid progression on the A $\beta$  network in PD and the relationship between the cognitive impairment and the alteration of topological measurements.

This is the first study demonstrating topological disorganization, characterized by a reduction in global efficiency and modularity and altered hub pattern, affecting network integration and impairing neural segregation in PD patients with A $\beta$  accumulation. These results are highly indicative of the spreading pattern of the A $\beta$  between modules and networks, providing more insights into the beta-amyloidopathy of PD.

**Author Contributions** Study conception and design: JK and APS

Data acquisition: CG and LC

Data analysis: JK and CG

Data interpretation: JK and APS

Manuscript drafting: JK

Manuscript review and critique for important intellectual content: JK, CG, SSC, AM, LC, MV, SH, and APS

Approved version to be published: JK and APS

**Funding Information** This work was supported by the Canadian Institutes of Health Research (MOP-136778). Dr. Antonio Strafella is supported by the Canada Research Chair Program.

### Compliance with Ethical Standards

**Conflict of Interest** The authors declare that they have no conflict of interest.

## References

1. Khoo TK, Yarnall AJ, Duncan GW, Coleman S, O'Brien JT, Brooks DJ, Barker RA, Burn DJ (2013) The spectrum of nonmotor symptoms in early Parkinson disease. *Neurology* 80(3):276–281
2. Valli M, Mihaescu A, Strafella AP (2017) Imaging behavioural complications of Parkinson's disease. *Brain Imaging Behav.* <https://doi.org/10.1007/s11682-017-9764-1>
3. Mattila P, Rinne J, Helenius H, Dickson DW, Røyttä M (2000) Alpha-synuclein-immunoreactive cortical Lewy bodies are associated with cognitive impairment in Parkinson's disease. *Acta Neuropathol* 100(3):285–290
4. Petrou M, Bohnen NI, Müller ML, Koeppe RA, Albin RL, Frey KA (2012) A $\beta$ -Amyloid deposition in patients with Parkinson disease at risk for development of dementia. *Neurology* 79(11):1161–1167
5. Klunk WE, Engler H, Nordberg A, Wang Y, Blomqvist G, Holt DP, Bergström M, Savitcheva I et al (2004) Imaging brain amyloid in Alzheimer's disease with Pittsburgh Compound-B. *Ann Neurol* 55(3):306–319
6. Mintun M, Larossa G, Sheline Y, Dence C, Lee SY, Mach R, Klunk W, Mathis C et al (2006) [11C] PIB in a nondemented population potential antecedent marker of Alzheimer disease. *Neurology* 67(3):446–452
7. Petrou M, Dwamena BA, Foerster BR, MacEachern MP, Bohnen NI, Müller ML, Albin RL, Frey KA (2015) Amyloid deposition in Parkinson's disease and cognitive impairment: a systematic review. *Mov Disord* 30(7):928–935. <https://doi.org/10.1002/mds.26191>
8. Maetzler W, Reimold M, Liepelt I, Solbach C, Leyhe T, Schweitzer K, Eschweiler GW, Mittelbronn M et al (2008) [11C]PIB binding in Parkinson's disease dementia. *Neuroimage* 39(3):1027–1033. <https://doi.org/10.1016/j.neuroimage.2007.09.072>
9. Edison P, Rowe CC, Rinne JO, Ng S, Ahmed I, Kempainen N, Villemagne VL, O'Keefe G et al (2008) Amyloid load in Parkinson's disease dementia and Lewy body dementia measured with [11C] PIB positron emission tomography. *J Neurol Neurosurg Psychiatry* 79(12):1331–1338
10. Gomperts SN, Locascio JJ, Rentz D, Santarlasci A, Marquie M, Johnson KA, Growdon JH (2013) Amyloid is linked to cognitive decline in patients with Parkinson disease without dementia. *Neurology* 80(1):85–91
11. Akhtar RS, Xie SX, Chen YJ, Rick J, Gross RG, Nasrallah IM, Van Deerlin VM, Trojanowski JQ et al (2017) Regional brain amyloid- $\beta$  accumulation associates with domain-specific cognitive performance in Parkinson disease without dementia. *PLoS One* 12(5):e0177924. <https://doi.org/10.1371/journal.pone.0177924>
12. Campbell MC, Markham J, Flores H, Hartlein JM, Goate AM, Cairns NJ, Videen TO, Perlmutter JS (2013) Principal component analysis of PiB distribution in Parkinson and Alzheimer diseases. *Neurology* 81(6):520–527. <https://doi.org/10.1212/WNL.0b013e31829e6f94>
13. Bullmore E, Sporns O (2009) Complex brain networks: graph theoretical analysis of structural and functional systems. *Nat Rev Neurosci* 10(3):186–198
14. Sporns O (2011) The human connectome: a complex network. *Ann N Y Acad Sci* 1224:109–125. <https://doi.org/10.1111/j.1749-6632.2010.05888.x>
15. Sepulcre J, Sabuncu MR, Becker A, Sperling R, Johnson KA (2013) In vivo characterization of the early states of the amyloid-beta network. *Brain* 136 (Pt 7):2239–2252. <https://doi.org/10.1093/brain/awt146>
16. Jiang J, Duan H, Huang Z, Yu Z, Alzheimer's Disease Neuroimaging I (2015) Study of amyloid-beta peptide functional brain networks in AD, MCI and HC. *Biomed Mater Eng* 26(Suppl 1):S2197–S2205. <https://doi.org/10.3233/BME-151525>
17. Duan H, Jiang J, Xu J, Zhou H, Huang Z, Yu Z, Yan Z, Initiative ADN (2017) Differences in A $\beta$  brain networks in Alzheimer's disease and healthy controls. *Brain Res* 1655:77–89
18. Pereira JB, Strandberg TO, Palmqvist S, Volpe G, van Westen D, Westman E, Hansson O, Initiative ADN (2017) Amyloid network topology characterizes the progression of Alzheimer's disease during the prodementia stages. *Cereb Cortex* 28(1):340–349
19. Defer GL, Widner H, Marié RM, Rémy P, Levivier M (1999) Core assessment program for surgical interventional therapies in Parkinson's disease (CAPSIT-PD). *Mov Disord* 14(4):572–584
20. Tomlinson CL, Stowe R, Patel S, Rick C, Gray R, Clarke CE (2010) Systematic review of levodopa dose equivalency reporting in Parkinson's disease. *Mov Disord* 25(15):2649–2653
21. Beck AT, Steer RA, Brown GK (1996) Manual for the Beck depression inventory-II. San Antonio: TX: Psychological Corporation.
22. Rusjan P, Mamo D, Ginovart N, Hussey D, Vitcu I, Yasuno F, Tetsuya S, Houle S et al (2006) An automated method for the extraction of regional data from PET images. *Psychiatry Res Neuroimaging* 147(1):79–89
23. Talairach J, Tournoux P (1988) Co-planar stereotaxic atlas of the human brain: 3-dimensional proportional system: an approach to cerebral imaging.
24. Logan J, Fowler JS, Volkow ND, Wang G-J, Ding Y-S, Alexoff DL (1996) Distribution volume ratios without blood sampling from graphical analysis of PET data. *J Cereb Blood Flow Metab* 16(5):834–840
25. Rowe CC, Ng S, Ackermann U, Gong SJ, Pike K, Savage G, Cowie T, Dickinson K et al (2007) Imaging  $\beta$ -amyloid burden in aging and dementia. *Neurology* 68(20):1718–1725
26. Lopresti BJ, Klunk WE, Mathis CA, Hoge JA, Ziolkowski SK, Lu X, Meltzer CC, Schimmel K et al (2005) Simplified quantification of Pittsburgh Compound B amyloid imaging PET studies: a comparative analysis. *J Nucl Med* 46(12):1959–1972
27. Knezevic D, Verhoeff NPL, Hafizi S, Strafella AP, Graff-Guerrero A, Rajji T, Pollock BG, Houle S et al (2018) Imaging microglial activation and amyloid burden in amnesic mild cognitive impairment. *J Cereb Blood Flow Metab* 38(11):1885–1895. <https://doi.org/10.1177/0271678X17741395>
28. Villeneuve S, Rabinovici GD, Cohn-Sheehy BI, Madison C, Ayakta N, Ghosh PM, La Joie R, Arthur-Bentil SK et al (2015) Existing Pittsburgh Compound-B positron emission tomography thresholds are too high: statistical and pathological evaluation. *Brain* 138(7):2020–2033. <https://doi.org/10.1093/brain/awv112>
29. Rubinov M, Sporns O (2010) Complex network measures of brain connectivity: uses and interpretations. *Neuroimage* 52(3):1059–1069
30. Hosseini SH, Hoefl F, Kesler SR (2012) GAT: a graph-theoretical analysis toolbox for analyzing between-group differences in large-scale structural and functional brain networks. *PLoS One* 7(7):e40709
31. He Y, Chen ZJ, Evans AC (2007) Small-world anatomical networks in the human brain revealed by cortical thickness from MRI. *Cereb Cortex* 17(10):2407–2419. <https://doi.org/10.1093/cercor/bhl149>
32. Seo EH, Lee DY, Lee J-M, Park J-S, Sohn BK, Lee DS, Choe YM, Woo JI (2013) Whole-brain functional networks in cognitively normal, mild cognitive impairment, and Alzheimer's disease. *PLoS One* 8(1):e53922
33. Achard S, Bullmore E (2007) Efficiency and cost of economical brain functional networks. *PLoS Comput Biol* 3(2):e17. <https://doi.org/10.1371/journal.pcbi.0030017>
34. Latora V, Marchiori M (2001) Efficient behavior of small-world networks. *Phys Rev Lett* 87(19):198701
35. Watts DJ, Strogatz SH (1998) Collective dynamics of 'small-world' networks. *Nature* 393(6684):440–442

36. Newman ME (2006) Finding community structure in networks using the eigenvectors of matrices. *Phys Rev E* 74(3):036104
37. Freeman LC (1978) Centrality in social networks conceptual clarification. *Soc Networks* 1(3):215–239
38. Wang T, Wang K, Qu H, Zhou J, Li Q, Deng Z, Du X, Lv F et al (2016) Disorganized cortical thickness covariance network in major depressive disorder implicated by aberrant hubs in large-scale networks. *Sci Rep* 6:27964
39. Bassett DS, Bullmore E (2006) Small-world brain networks. *Neuroscientist* 12:512–523. <https://doi.org/10.1177/1073858406293182>
40. Ramsay JO, Dalzell CJ (1991) Some tools for functional data analysis. *J R Stat Soc Ser B Methodol* 53(3):539–572
41. Kotagal V, Bohnen NI, Müller ML, Frey KA, Albin RL (2017) Cerebral amyloid burden and Hoehn and Yahr stage 3 scoring in Parkinson disease. *J Park Dis* 7(1):143–147
42. Dyrba M, Mohammadi A, Grothe MJ, Kirste T, Teipel SJ (2018) Assessing inter-modal and inter-regional dependencies in prodromal Alzheimer's disease using multimodal MRI/PET and Gaussian graphical models. *arXiv preprint arXiv:180400049*
43. Yang J, Hu C, Guo N, Dutta J, Vaina LM, Johnson KA, Sepulcre J, Fakhri GE et al (2017) Partial volume correction for PET quantification and its impact on brain network in Alzheimer's disease. *Sci Rep* 7(1):13035. <https://doi.org/10.1038/s41598-017-13339-7>
44. Thal DR, Rüb U, Orantes M, Braak H (2002) Phases of A $\beta$ -deposition in the human brain and its relevance for the development of AD. *Neurology* 58(12):1791–1800
45. Sporns O, Honey CJ, Kötter R (2007) Identification and classification of hubs in brain networks. *PLoS One* 2(10):e1049
46. Leyton CE, Cassidy B, Villemagne VL, Jones G, Kwok JB, Rowe CC, Ballard KJ, Piguet O et al (2016) Divergent network patterns of amyloid- $\beta$  deposition in logopenic and amnesic Alzheimer's disease presentations. *Biol Psychiatry Cogn Neurosci Neuroimaging* 1(1):24–31
47. Culham JC, Cavina-Pratesi C, Singhal A (2006) The role of parietal cortex in visuomotor control: what have we learned from neuroimaging? *Neuropsychologia* 44(13):2668–2684
48. Garcia-Diaz AI, Segura B, Baggio HC, Marti MJ, Valdeoriola F, Compta Y, Bargallo N, Uribe C et al (2018) Structural brain correlations of visuospatial and visuoperceptual tests in Parkinson's disease. *J Int Neuropsychol Soc* 24(1):33–44

**Publisher's Note** Springer Nature remains neutral with regard to jurisdictional claims in published maps and institutional affiliations.